Enhanced Radio-SLAM Algorithm Using Building Geometry Constraints

Zhen Lyu[1], Guohao Zhang[1,*]

[1]The Hong Kong Polytechnic University, 11 Yuk Choi Road, Hong Kong

Abstract

Wi-Fi-based radio-SLAM (simultaneous localization and mapping) estimates the positions of users and access points (APs) simultaneously in GPS-denied indoor environments. To address the observability degradation in radio-SLAM caused by using only relative distance measurements between APs and the user, this paper proposes a positioning method based on the extended Kalman filter (EKF) and global geometry constraints. This method first uses the relationship between signal strength and ranging in the free space path loss (FSPL) model to determine the visibility of the AP. Then, it establishes a globally constrained positioning framework by integrating AP's observed visibility and estimated visibility (from the estimated results of the geometric collision detection of walls). Simulation results show the improvement of our positioning methods, compared with the traditional EKF, the proposed method improves user positioning accuracy (RMSE) by 34%, and AP location estimation accuracy by 37%, enhancing users' perception capability in unknown environments.

Keywords

Indoor positioning, Wi-Fi RTT, visibility matching, EKF

1. Introduction

With the rapid growth in indoor location-based services, wireless signal-based indoor positioning technologies have become crucial solutions in GPS-denied environments [1, 2]. The fine-time measurement protocol launched in IEEE 802.11 mc for indoor positioning accelerated the research related to Wi-Fi-based indoor positioning.

However, existing systems generally rely on pre-deployed access points (APs) with known locations, which faces significant challenges in practical applications. Traditional approaches relying on known AP locations, such as trilateration [3] and fingerprint matching [4], not only require complete prior knowledge of AP positions but also cannot adapt to dynamic environments with moving or newly added APs. Fingerprint also demands extensive manual effort for offline calibration and struggles with routine alterations like furniture rearrangement. Temporarily deployed mobile APs, or unrecorded APs in older buildings, can completely undermine conventional positioning methods. Meanwhile, complex indoor environments with multipath effects [5] and non-line-of-sight (NLOS) [6] propagation can severely degrade the accuracy of ranging measurements based on round-trip time (RTT) and received signal strength (RSSI), ultimately compromising the reliability of the entire positioning system.

These real-world challenges urgently call for innovative solutions that can achieve precise positioning even when AP locations are unknown. On the other hand, wireless positioning methods based on simultaneous localization and mapping (SLAM) can estimate both user and AP positions simultaneously, also known as radio-SLAM [7]. Barneto et al. [8] introduce a novel state model for mapping signal diffuse and specular scattering, which allows efficient tracking of individual scatterers over time using interacting multiple model (IMM) extended Kalman filter and smoother. Leitinger et al. [9] formulated the SLAM problem within a Bayesian framework, representing it as a factor graph to enable efficient margi nalization of the joint posterior distribution through belief propagation (BP). However, for Kalman filter-based approaches and factor graph techniques [10], the system has poor observability

IPIN-WCAL 2025: Workshop for Computing & Advanced Localization at the Fifteenth International Conference on Indoor Positioning and Indoor Navigation, September 15–18, 2025, Tampere, Finland

zhenn.lyu@connect.polyu.hk (Z. Lyu); gh.zhang@polyu.edu.hk (G. Zhang)

0009-0006-5212-8307 (Z. Lyu); 0000-0002-4661-9058 (G. Zhang)

when simultaneously estimating both agent and AP positions using only relative distance measurements between them. Morales's research [11] shows that in such radio-SLAM system, poor observability can cause the clock biases of the receiver and transmitter to be random and unobservable, and the estimated error variance to diverge. As a result, the lack of global constraints leads to translational and rotational errors in the estimated localization results. Existing research has not fully utilized the important prior information contained in building floor plans to enhance the physical consistency of the solution.

To address the challenges, this paper proposes an innovative radio-SLAM framework by integrating signal transmission characteristics with environmental structural constraints. Our contributions are:

- proposes an observed visibility classification method based on joint analysis of RTT and RSSI. By thoroughly examining the residual between these two measurements, we can identify LOS and NLOS propagation states.
- introduces geometric constraints from building floor plans. Rather than simply adjusting noise variance based on visibility, we leverage the consistency between the estimated user-AP relative visibility and the prior map's visibility information.

2. Visibility classification

In a LOS environment, the RSSI and RTT distance measurement should conform to the FSPL model; if there is occlusion, RSSI will be significantly lower than the theoretical value due to additional attenuation. The residual y of the measurement RSSI and predicted RSSI based on FSPL is used to determine the visibility. If $y < T$, the signal is determined as an LOS signal. Otherwise, the signal is a NLOS signal. T is the dynamic threshold determined by different environments, $T = K \cdot \sigma$.

$$V_O = \begin{cases} \text{LOS}, & \text{if } y < T, \\ \text{NLOS}, & \text{if } y \geq T. \end{cases} \tag{1}$$

In terms of the estimated visibility, it is determined by whether the line from the user and AP intersects with the wall derived from the floor plan[3]. Expressed as:

$$V_E = \begin{cases} \text{NLOS}, & \text{if } \vec{pp}^j \text{and } \mathbf{L} \text{ intersect}, \\ \text{LOS}, & \text{if } \vec{pp}^j \text{and } \mathbf{L} \text{ do not intersect}, \end{cases} \tag{2}$$

where $\vec{pp}^j$ is the line segments connecting estimated user $p = (x, y)$ and AP locations $p^j = (x^j, y^j)$, $\mathbf{L}$ is the vector set of the wall. Therefore, the consistency of visibility is:

$$V_C = \text{XNOR}(V_O, V_E), \tag{3}$$

where the XNOR operation returns true only when both inputs are equal.

3. System Modeling

Distance measurement is a nonlinear equation of AP and user locations. We choose the Extended Kalman Filter (EKF) to solve the nonlinear problem through local linearization. The nonlinear prediction equation and measurement equation are differentiated and linearized by replacing the tangent line. It is a first-order Taylor expansion at the mean.

The state vector contains the user's position (x, y), user's velocity $(\dot{x}, \dot{y})$ and the positions of J APs (x^j, y^j):

$$\mathbf{x} = \begin{bmatrix} x & y & \dot{x} & \dot{y} & x^1 & y^1 & \cdots & x^J & y^J \end{bmatrix}^T \in \mathbb{R}^{2J+4}. \tag{4}$$

The status prediction is:

$$\hat{\mathbf{x}}_{k|k-1} = \mathbf{F}_k \hat{\mathbf{x}}_{k-1|k-1}, \tag{5}$$

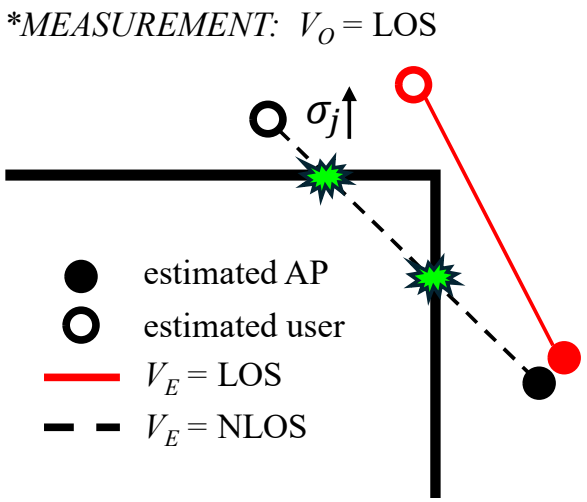

Figure 1: The example of LOS and NLOS propagation of V_E. When the V_O and V_E are inconsistent, the weight of the corresponding AP measurement value on the EKF positioning result will decrease.

where $\mathbf{x}_{k-1|k-1}$ is the posterior state at $k-1$, $\mathbf{x}_{k|k-1}$ is the prior state, $\mathbf{F}_k \in \mathbb{R}^{(2J+4)\times(2J+4)}$ is the state transition Jacobian matrix:

$$\mathbf{F}_k = \left.\frac{\partial f}{\partial \mathbf{x}}\right|_{\hat{\mathbf{x}}_{k-1|k-1}} = \begin{bmatrix} 1 & 0 & \Delta t & 0 & 0 & \cdots & 0 \\ 0 & 1 & 0 & \Delta t & 0 & \cdots & 0 \\ 0 & 0 & 1 & 0 & 0 & \cdots & 0 \\ 0 & 0 & 0 & 1 & 0 & \cdots & 0 \\ 0 & 0 & 0 & 0 & \mathbf{I}_{2J} & \cdots & 0 \\ \vdots & \vdots & \vdots & \vdots & \vdots & \ddots & \vdots \\ 0 & 0 & 0 & 0 & 0 & \cdots & \mathbf{I}_{2J} \end{bmatrix}. \quad (6)$$

The covariance prediction is:

$$\mathbf{P}_{k|k-1} = \mathbf{F}_k \mathbf{P}_{k-1|k-1} \mathbf{F}_k^T + \mathbf{Q}_k, \quad (7)$$

where $\mathbf{Q}_k$ is defined as

$$\mathbf{Q}_k = \mathrm{diag}\left(\sigma_x^2,\ \sigma_y^2,\ \sigma_{\dot{x}}^2,\ \sigma_{\dot{y}}^2,\ \sigma_{x1}^2, \sigma_{y1}^2,\ \ldots,\ \sigma_{xj}^2, \sigma_{yj}^2\right), \quad (8)$$

corresponding to different variances of the status. The residuals to the measurement value $\mathbf{z}_k$ is:

$$\mathbf{y}_k = \mathbf{z}_k - \mathbf{H}_k \hat{\mathbf{x}}_{k|k-1}, \quad (9)$$

where the measurement Jacobian matrix $\mathbf{H}_k$ is:

$$\mathbf{H}_k = \left.\frac{\partial h}{\partial \mathbf{x}}\right|_{\hat{\mathbf{x}}_{k|k-1}} = \begin{bmatrix} \frac{\partial d^1}{\partial x} & \frac{\partial d^1}{\partial y} & 0 & 0 & \cdots & \frac{\partial d^1}{\partial y^J} \\ \frac{\partial d^2}{\partial x} & \frac{\partial d^2}{\partial y} & 0 & 0 & \cdots & \frac{\partial d^2}{\partial y^J} \\ \vdots & \vdots & \vdots & \vdots & \ddots & \vdots \\ \frac{\partial d^J}{\partial x} & \frac{\partial d^J}{\partial y} & 0 & 0 & \cdots & \frac{\partial d^J}{\partial y^J} \end{bmatrix}. \quad (10)$$

The measurement prediction function is :

$$\begin{bmatrix} d^1 \\ d^2 \\ \vdots \\ d^J \end{bmatrix} = \begin{bmatrix} \sqrt{(x-x^1)^2 + (y-y^1)^2} \\ \sqrt{(x-x^2)^2 + (y-y^2)^2} \\ \vdots \\ \sqrt{(x-x^J)^2 + (y-y^J)^2} \end{bmatrix}. \quad (11)$$

The Kalman gain is:

$$\mathbf{K}_k = \mathbf{P}_{k|k-1}\mathbf{H}_k^T(\mathbf{H}_k\mathbf{P}_{k|k-1}\mathbf{H}_k^T + \mathbf{R}_k)^{-1}, \tag{12}$$

where

$$\mathbf{R}_k = \text{diag}\Big(\sigma_{d1}^2, ..., \sigma_{dj}^2\Big), \tag{13}$$

corresponding to the variances of measurements. Considering the influence of visibility consistency,

$$\sigma_{dj} = \begin{cases} \sigma_{dj}, & \text{if } V_C = 1 \\ D \cdot \sigma_{dj}, & \text{if } V_C = 0, \end{cases} \tag{14}$$

where D is the trust scaling factor, if visibility is inconsistent, the corresponding measurement value has higher noise variance. The state and covariance update is:

$$\hat{\mathbf{x}}_{k|k} = \hat{\mathbf{x}}_{k|k-1} + \mathbf{K}_k\mathbf{y}_k, \tag{15}$$

$$\mathbf{P}_{k|k} = (\mathbf{I} - \mathbf{K}_k\mathbf{H}_k)\mathbf{P}_{k|k-1}. \tag{16}$$

In our framework, the visibility consistency of APs serves as a reliability indicator for measurement validation. Specifically, when visibility consistency is satisfied, the corresponding AP's measurements are deemed more trustworthy, and we proceed with standard state update and prediction following the EKF workflow. Figure 1 shows an example of this process. Assume that, based on RSSI and RTT, V_O is classified as LOS. If the segment connecting AP and user intersects the wall, V_E is NLOS, which is inconsistent compared to V_O. Therefore, this measurement value is unreliable, and the value of the element of the measurement noise covariance matrix of AP increases.

4. Evaluation

The performance of the proposed EKF algorithm is verified by simulation in a dynamic noise environment and compared with other filtering methods.

4.1. Experimental setting

We set the positions of the walls $\mathbf{L}$, the location of the AP ($([-3, 5], [30, 5], [15, 20])$ with the unit as meters), and the trajectory of the user. The user's movement consists of straight walking and turning, distributed in different rooms within 120 seconds.

All parameter settings used in the system and the initial settings of EKF are shown in Table 1.

Table 1
System Parameters

Parameters	**Value**
J	3
K	3
Δt	0.1 s
σ_x, σ_y	0.1 m
$\sigma_{\dot{x}}, \sigma_{\dot{y}}$	0.5 m
σ_{xj}, σ_{yj}	10^{-6} m
σ_d	1.5 m
D	10
Initial State	**Value**
$\mathbf{x}_0$	$[1, 14, 1, 0, 0, 2, 25, 0, 22, 25]^T$
$\mathbf{P}_0$	$\text{diag}([5, 5, 1, 1, 20, 20, 20, 20, 20, 20])$

4.2. Results and Analysis

Figure 2 shows the result of EKF and the proposed visibility-assisted positioning method. Figure 2(a) shows the trajectory of the result.

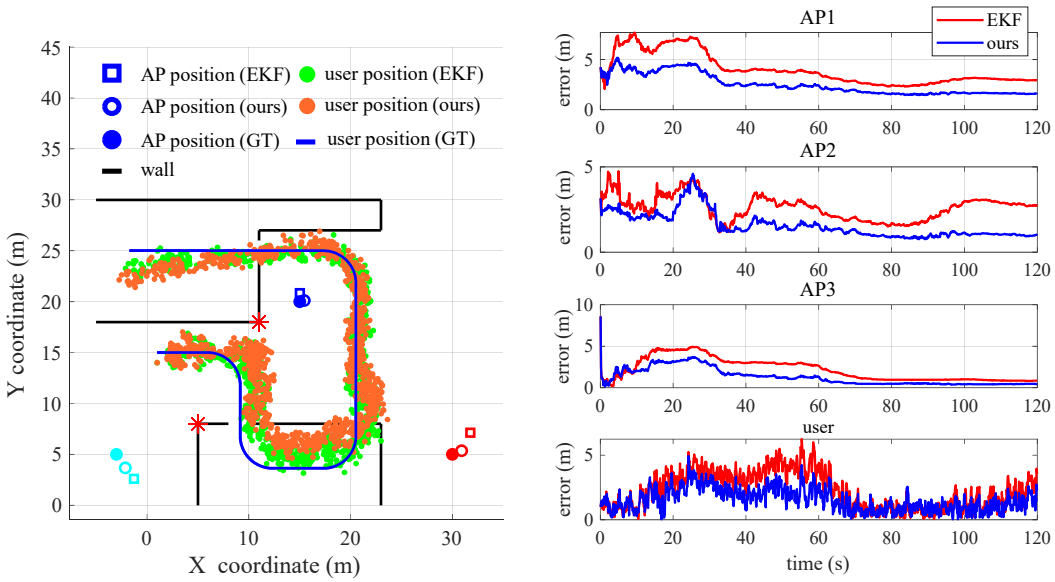

(a) The result of EKF and the proposed visibility-assisted positioning method. The red dots indicate the position-ing result of the EKF, and the green dots indicate the positioning result of the proposed method.

(b) The error comparison of different APs and the user. The red line is the estimated error of EKF, and the blue line is the estimated error of our method.

Figure 2: Positioning trajectory and accuracy.

To analyze the time-error results of our method versus traditional EKF in estimating the positions of the user and three APs, we plotted all curves in the same coordinate system to observe overall trends (Figure 2(b)). The obvious difference between our method and EKF is that the measurement variance matrix is adjusted based on the visibility—— rather than simply adjusting noise variance based on visibility, we leverage the consistency between the estimated user-AP relative visibility and the prior map's visibility information. While our method does not exhibit significantly faster convergence than EKF for user positioning, the visibility constraints mitigate the initial positioning error amplification caused by biased initial values. After convergence, our method achieves lower steady-state errors. Additionally, the AP error curves demonstrate that our method exhibits smaller oscillations and positioning errors. Quantitative comparisons of key metrics (see Table 2) further confirm our advantages.

Table 2
Performance Comparison (EKF / Proposed Method)

Metrics	User	AP1	AP2	AP3
Error Mean (m)	2.26 / 1.52	3.97 / 2.48	2.61 / 1.57	2.16 / 1.26
Error Max (m)	6.24 / 4.93	7.68 / 5.19	4.75 / 4.60	8.60 / 8.60
Error Std (m)	1.41 / 0.88	1.53 / 1.01	0.71 / 0.74	1.35 / 1.01
Error RMSE (m)	2.66 / 1.76	4.25 / 2.68	2.71 / 1.73	2.55 / 1.61

The comparative analysis demonstrates that our proposed method significantly outperforms the conventional EKF across most metrics. For positioning accuracy, the mean error improved by 32.7% (from $2.26m$ to $1.52m$) for user localization and up to 41.7% (from $2.16m$ to $1.26m$) for AP3. The RMSE showed consistent enhancements, particularly for AP1 with 36.9% reduction (from $4.25m$ to $2.68m$).

Regarding error stability, the standard deviation decreased by 37.6% (from $1.41m$ to $0.88m$) for user positioning, though AP2 exhibited a marginal 4.2% increase (from $0.71m$ to $0.74m$). Notably, the unchanged maximum error for AP3 ($8.60m$) is attributed to initial value deviation at $k = 1$, suggesting the algorithm's sensitivity to initialization. The results confirm our method's superior performance in both accuracy and consistency, while highlighting the need for improved initialization techniques to address outlier cases.

The superior positioning accuracy achieved by our method stems fundamentally from its dynamic adaptation of the measurement noise covariance matrix $\mathbf{R}_k$ in the EKF framework. Specifically, our approach innovatively integrates RSSI/RTT ranging data with posterior visibility verification to establish a dual reliability validation mechanism: when an AP's observed visibility (based on signal characteristics) aligns with its geometric visibility (determined by intersection tests between estimated positions and walls), the data is deemed reliable and corresponding σ_{dj} in $\mathbf{R}_k$ remains unchanged; when discrepancies occur (e.g., signal-indicated LoS conflicts with geometric occlusion), corresponding σ_{dj} in $\mathbf{R}_k$ is increased to reduce that AP's influence. This design fundamentally overcomes the limitations of the traditional EKF in complex environments due to the fixed noise assumption. It integrates environmental information as constraints through a plan view, automatically suppresses interference from unreliable measurements in scenes with inconsistent visibility, and further improves positioning accuracy.

5. Conclusion

To address the issue of insufficient global constraints in AP position estimation for radio-SLAM, this paper proposes an EKF-based localization method leveraging visibility consistency. By integrating the observed and estimated visibility of APs, the method establishes geometric constraints to enhance global accuracy. Simulation results demonstrate that the proposed residual-based visibility discrimination approach effectively distinguishes between LOS and NLOS signals. In terms of positioning accuracy, multiple evaluation metrics, including RMSE, mean error, and standard deviation, show significant improvements. This work introduces a novel approach by incorporating global geometric constraints when only relative distance measurements of the target parameters are available, offering a new solution for sensor network node calibration in an environment with mobile devices.

However, the positioning results are sensitive to initial values, and the measurement data is more unstable in indoor environments with severe multipath effects. Future research will focus on developing more robust initial value calibration algorithms and conducting experiments to evaluate the accuracy and stability of our method.

Declaration on Generative AI

During the preparation of this work, the author(s) used Chat-GPT-4 in order to: Grammar and spelling check. After using these tool(s)/service(s), the author(s) reviewed and edited the content as needed and take(s) full responsibility for the publication's content.

References

[1] M. Youssef, A. Agrawala, The horus wlan location determination system, in: Proceedings of the 3rd international conference on Mobile systems, applications, and services, 2005, pp. 205–218.

[2] J. Hyun, T. Oh, H. Lim, H. Myung, Uwb-based indoor localization using ray-tracing algorithm, in: 2019 16th International Conference on Ubiquitous Robots (UR), IEEE, 2019, pp. 98–101.

[3] Z. Lyu, S. Bai, X. Wang, L. Li, G. Zhang, Wi-fi rtt indoor positioning using visibility matching with nlos receptions, IEEE Internet of Things Journal (2025).

[4] K. Kaemarungsi, P. Krishnamurthy, Modeling of indoor positioning systems based on location fingerprinting, in: Ieee Infocom 2004, volume 2, IEEE, 2004, pp. 1012–1022.

[5] H. Liu, H. Darabi, P. Banerjee, J. Liu, Survey of wireless indoor positioning techniques and systems, IEEE Transactions on Systems, Man, and Cybernetics, Part C (Applications and Reviews) 37 (2007) 1067–1080.

[6] E. Zola, I. Martin-Escalona, Ieee 802.11 mc ranging performance in a real nlos environment, in: 2021 17th International Conference on Wireless and Mobile Computing, Networking and Communications (WiMob), IEEE, 2021, pp. 377–384.
[7] B. Amjad, Q. Z. Ahmed, P. I. Lazaridis, M. Hafeez, F. A. Khan, Z. D. Zaharis, Radio slam: A review on radio-based simultaneous localization and mapping, IEEE Access 11 (2023) 9260–9278.
[8] C. B. Barneto, E. Rastorgueva-Foi, M. F. Keskin, T. Riihonen, M. Turunen, J. Talvitie, H. Wymeersch, M. Valkama, Millimeter-wave mobile sensing and environment mapping: Models, algorithms and validation, IEEE Transactions on Vehicular Technology 71 (2022) 3900–3916.
[9] E. Leitinger, F. Meyer, F. Hlawatsch, K. Witrisal, F. Tufvesson, M. Z. Win, A belief propagation algorithm for multipath-based slam, IEEE transactions on wireless communications 18 (2019) 5613–5629.
[10] S. Bai, W. Wen, D. Su, L.-T. Hsu, Graph-based indoor 3d pedestrian location tracking with inertial-only perception, IEEE Transactions on Mobile Computing (2025).
[11] J. J. Morales, Z. M. Kassas, Stochastic observability and uncertainty characterization in simultaneous receiver and transmitter localization, IEEE Transactions on Aerospace and Electronic Systems 55 (2018) 1021–1031.